ELSEVIER

Chemical Engineering Journal 71 (1998) 233–242

Chemical Engineering Journal

Modeling of coal combustion and NO_x formation in a W-shaped boiler furnace

J.R. Fan*, J. Jin, X.H. Liang, L.H. Chen, K.F. Cen

Department of Energy Engineering, Zhejiang University, Hangzhou, 310027, China

Received 11 February 1998; received in revised form 21 August 1998; accepted 8 September 1998

Abstract

A numerical model for the gas-particle flow dynamics has been combined with a NO_x – chemistry post-processor to predict the formation of nitric oxide in a three-dimensional, W-shaped boiler furnace burning pulverized fuel. The model includes the complex interaction of gas-particle turbulent flow, heat transfer, gaseous chemical reaction, coal combustion, and NO_x reaction chemistry. Because the fuel nitrogen is released in proportion to the burnout of the pulverized coal particles, the particles are treated in a Lagrangian framework in order to track burning pulverized coal particles through the gas continuum. The results show the capability of the model for describing NO_x emissions under different operating conditions for full and partial load.

Keywords: Nitric oxide; Pulverized fuel; Gas particle flow

1. Introduction

The combustion of pulverized coal in utility boilers leads to the formations of nitrogen oxides (NO_x). The emissions of NO_x contribution to the formation of acid rain and the production of photochemical smog. The need to control pollutant emissions from coal-fired plants has been recognized internationally. Approaches to controlling emission vary from region to region and from country to country. Many studies have appeared and several reviews have been presented [1,2].

W-shaped boiler furnaces are suitable to burn anthracite and low-volatile-matter coals and the combustion is stale at low loads. These systems have higher combustion efficiencies than tangentially-fired boilers because of longer flame lengths and high coal-to-air ratios for the primary mixtures feeding the second combustion stage. W-shaped boilers equipped with low NO_x swirl burners can reduce emissions of NO_x.

Concentration levels of NO_x depend on a number of factors e.g., rank of coal, burner type, flame temperature, mixing intensity with air, firing intensity, coal particle size and functional forms of nitrogen in the coal. The prediction of NO_x formation in turbulent, pulverized coal systems is very complex because of the large number of reactions that are required to describe this process and the turbulent flow in practical systems. The modeling of the NO_x formation from coal flames is usually based on the mechanism proposed by De Soete for the nitrogen from volatiles [3]. Several investigators have attempted to use a correlation-type approach to predict NO_x levels from furnace operational and coal parameters [4]. Smouse et al. [5] used a neural network approach on a set of 69 tests in tangentially fired furnaces. Although an alternative NO_x modeling approach, in which the full set of nitrogen-chemistry equations contains of the order of 100 identified elementary reactions, has been used to predict NO_x levels, it is not currently practical to solve this set combined with a complex gas-particle fluid dynamics model [6]. Therefore, the simplified approach uses a post-processor NO_x chemistry model in conjunction with a gas-particle fluid dynamics model [7–10]. Many attempts have been made to predict NO_x formation in tangential fired boilers or in front wall fired boilers [11–13]. However it is impossible to find in the literature a well-documented numerical simulation of NO_x formation in a three-dimensional, W-shaped boiler furnace.

The purpose of our research has been to investigate numerically the characteristics of gas-particle turbulent flow, heat transfer, gaseous chemical reaction, coal combustion, and NO_x formation in a large-scale, W-shaped boiler

*Corresponding author.: Fax: +86-571-795-1358; e-mail: fanjr@public.hz.zj.cn

1385-8947/98/$ – see front matter
PII: S1385-8947(98)00130-2

furnace equipped with low NO_x swirl burners under different operational conditions. The numerical model is briefly described in the next section as well as a simplified post-processor approach to calculate NO_x emissions. The numerical results discussed in the following section show the main differences between operational conditions for full load (design case) and partial load. The data resulting from the present study provide a useful basis for designing W-shaped boiler furnaces.

2. Mathematical model

The gas-phase is described by elliptic, partial differential, conservation equations for a Newtonian fluid in 3-D Cartesian coordinates. The gas-phase conservation equations are solved for ten variables (ϕ): fluid pressure (p), three velocity components (u, v, w), enthalpy (h), concentration of the kth chemical species (Y_k), scalar mixture fraction (f),the time-mean value of square of difference of instantaneous mixture fraction (g), turbulent kinetic energy (k), and turbulent dissipation (ε). The Reynolds stress terms in the conservation equations are approximated using the eddy viscosity of Boussinesq. The standard two-equation k–ε model is used to calculate the turbulent viscosity. It is assumed that the equilibrium gas-phase chemistry, and the coupled turbulent flow field with chemical reactions may be described by the eddy-break-up model [14]. Convective and radiative heat transfer are also modeled. The latter by using the Monte Carlo method [15]. The general form of the elliptic differential equations for the gas-phase is given by

$$\mathrm{div}(\rho \boldsymbol{v}\phi) - \mathrm{div}(\Gamma\, \mathrm{grad}\phi) = S_\phi + S_{\phi,\mathrm{p}} \tag{1}$$

and the source terms of the gas-phase, S_ϕ, the dispersed phase, $S_{\phi,\mathrm{p}}$, and the effective viscosity, Γ_ϕ, are summarized in Table 1 for the different variables, ϕ. The source terms relating to NO_x chemistry are defined later.

The particle phase is treated by solving Lagrangian equations for the trajectories of a statistically significant sample of individual particles parcels, which represent a number of real particles with the same properties. Motion of the particles is determined by fluctuating velocity derived from a stochastic model developed by Fan et al. [16]. Particle trajectories are tracked throughout the computational domain, and interactions between the particles and gas are incorporated by an exchange of source terms for mass, momentum and energy. Coal particles are assumed to be composed of raw coal, char, ash, and moisture. Coal evolution is described in sequence by drying, devolatilization and char combustion, considering the particle diameter constant but the density variable. Coal-devolatilization and char-oxidation steps are considered. Coal devolatilization is modeled by a two-step mechanism. The gas formed from coal devolatilization participates in the gaseous reactions. The residual char particles are taken to be spherical and to burn under the control of a combination of external oxygen transfer and internal kinetic rates.

The conservation equations for particles are different in form from Eq. (1) and will now be summarized. The particle

Table 1
Eulerian conservation equations and identification of terms in Eq. (1)

ϕ	Γ	S_ϕ
1	0	$S_{\mathrm{p},m}$
u	μ_{eff}	$-\frac{\partial p}{\partial x}+\frac{\partial}{\partial x}\left(\mu_{\mathrm{eff}}\frac{\partial u}{\partial x}\right)+\frac{\partial}{\partial y}\left(\mu_{\mathrm{eff}}\frac{\partial v}{\partial x}\right)+\frac{\partial}{\partial z}\left(\mu_{\mathrm{eff}}\frac{\partial w}{\partial x}\right)+S_{\mathrm{p},u}$
v	μ_{eff}	$-\frac{\partial p}{\partial y}+\frac{\partial}{\partial x}\left(\mu_{eff}\frac{\partial u}{\partial y}\right)+\frac{\partial}{\partial y}\left(\mu_{\mathrm{eff}}\frac{\partial v}{\partial y}\right)+\frac{\partial}{\partial z}\left(\mu_{\mathrm{eff}}\frac{\partial w}{\partial y}\right)+S_{\mathrm{p},v}$
w	μ_{eff}	$-\frac{\partial p}{\partial z}+\frac{\partial}{\partial x}\left(\mu_{\mathrm{eff}}\frac{\partial u}{\partial z}\right)+\frac{\partial}{\partial y}\left(\mu_{\mathrm{eff}}\frac{\partial v}{\partial z}\right)+\frac{\partial}{\partial z}\left(\mu_{\mathrm{eff}}\frac{\partial w}{\partial z}\right)+S_{\mathrm{p,w}}$
k	$\mu_{\mathrm{eff}}/\sigma_{\mathrm{k}}$	$G_k-\rho\varepsilon+S_{\mathrm{p},k}$
ε	$\mu_{\mathrm{eff}}/\sigma_\varepsilon$	$\frac{\varepsilon}{k}(C_1G_k+C_2\varepsilon)+S_{\mathrm{p},\varepsilon}$
h	$\mu_{\mathrm{eff}}/\sigma_{\mathrm{h}}$	$\mathrm{div}(q_{\mathrm{r}})+S_{\mathrm{p,h}}$
Y_k	$\mu_{\mathrm{eff}}/\sigma_{\mathrm{s}}$	$-\sum_{j=1}^{ij}(\alpha'_{kj}-\alpha''_{kj})(R_j-R_{-j})+S_{p,Y_k}$
f	$\mu_{\mathrm{eff}}/\sigma_{\mathrm{f}}$	0
g	$\mu_{\mathrm{eff}}/\sigma_{\mathrm{g}}$	$G_{\mathrm{g}}-G_{\mathrm{g}_2}\rho\varepsilon g/k$

$$G_k=\mu_{\mathrm{eff}}\left\{2\left[\left(\frac{\partial u}{\partial x}\right)^2+\left(\frac{\partial v}{\partial y}\right)^2+\left(\frac{\partial w}{\partial z}\right)^2\right]+\left(\frac{\partial u}{\partial y}+\frac{\partial v}{\partial x}\right)^2+\left(\frac{\partial v}{\partial z}+\frac{\partial w}{\partial y}\right)^2+\left(\frac{\partial w}{\partial x}+\frac{\partial u}{\partial z}\right)^2\right\},$$

$$G_g=C_{g_1}\mu_{\mathrm{eff}}\left[\left(\frac{\partial f}{\partial x}\right)^2+\left(\frac{\partial f}{\partial y}\right)^2+\left(\frac{\partial f}{\partial z}\right)^2\right],\ \mu_{\mathrm{eff}}=\mu_t+\mu,\ \mu_t=C_\mu\rho k^2/\varepsilon,$$

$C_\mu=0.09, C_1=1.44, C_2=1.92, C_{\mathrm{g}_1}=2.8,\ C_{\mathrm{g}_2}=2.0, \sigma_k=1.0, \sigma_\varepsilon=1.3,$
$\sigma_h=1.0,\ \sigma_s=1.0,\ \sigma_f=0.7,\ \sigma_g=0.7$

mass-conservation equation is

$$\frac{dm_p}{dt} = -r_p \tag{2}$$

The equation of motion of a particle is

$$m_p\left(\frac{d\boldsymbol{v}_p}{dt}\right) = \frac{1}{2}\rho C_D(\boldsymbol{v}_g - \boldsymbol{v}_p)|\boldsymbol{v}_g - \boldsymbol{v}_p|A_p + m_p g \tag{3}$$

The conservation of particle energy is

$$m_p\left(\frac{dh_p}{dt}\right) = Q_c + Q_r + r_w L_w + r_v \Delta h_v + r_h Q_h \tag{4}$$

Diffusion-limited vaporization of moisture from the coal particle is described by

$$r_w = \frac{M_w \mathrm{Nu}_m C_g D_{wm} A_p (X_{wp} - X_{wg})}{d_p(1 - X_{wp} r_p / r_w)} \tag{5}$$

Fu et al. [17] use the equations

$$\frac{dV}{dt} = (V'_{daf} - V)K\exp(E/RT) \tag{6}$$

$$V'_{daf} = QV_{daf} \tag{7}$$

to describe the formation of volatile matter from coal dust.

Char is produced in competition with volatiles production as expressed by

$$r_{hm} = \frac{r_v(1 - Y_m)}{Y_m} \tag{8}$$

Char is assumed to be oxidized heterogeneously by a gaseous oxidizer that diffuses to the particle, is adsorbed, reacts with carbon, and is then described as CO. The char oxidizing rate is

$$r_{hl} = \frac{(A_p n_p)^2 M_{hp} m_g \phi_l K_{cpl} K_{pl} \xi_p C_{og} C_g}{M_g A_p n_p C_g(\xi_p K_{pl} + K_{cpl}) + r_p} \tag{9}$$

The total reaction rate for the coal particle is

$$r_p = r_v + r_{hl} + r_w \tag{10}$$

The carbon reaction rate is

$$r_h = r_{hm} - r_{hl} \tag{11}$$

The convection heat transfer rate to a spherical particle is quantified by the Nusselt number

$$\mathrm{Nu} = \frac{Q_c d_p}{A_p K_g (T_g - T_p)} \tag{12}$$

where $\mathrm{Nu} = 2 + 0.654\mathrm{Re}^{0.5}\mathrm{Pr}^{1/3}$. The radiative heat transfer to a particle of diameter d_p is given by

$$Q_r = \varepsilon\pi d_p^2\left(I - \sigma T_p^4\right) \tag{13}$$

Computations of char-oxidation rates require oxidizer mass-transfer rates from the bulk gas to the particle surface. The mass-transfer coefficient to spheres in the absence of surface transpiration effects is

$$\mathrm{Sh} = 2 + 0.654\,\mathrm{Re}^{0.5}\,\mathrm{Sc}^{1/3} \tag{14}$$

A simple model for nitrogen chemistry has been included in the mathematical model. Both the thermal and fuel mechanism are taken into account for NO_x formation. The prompt NO_x is neglected because it has been shown to form in insignificant amounts.

Thermal NO_x is assumed to form by a Zeldovich mechanism as shown in reactions as follows

$$N_2 + O \xrightarrow{k_1} NO + N \quad \text{(reaction 1)}$$

$$O_2 + N \xrightarrow{k_2} NO + O \quad \text{(reaction 2)}$$

The formation rate of NO from atmospheric nitrogen is

$$R_{N_2\to NO} = \frac{3\times 10^{14}\rho_g^{1.5} Y_{N_2} Y_{O_2}^{0.5}\exp(-65300/T_g) M_{NO}}{M_{N_2} M_{O_2}^{0.5}} \tag{15}$$

Thermal NO is formed by oxidation of atmospheric molecular nitrogen and is generally described by the Zeldovich or modified Zeldovich mechanism. These reactions are highly dependent on temperature and equivalence ratio, and NO formation by this mechanism is significantly reduced in fuel-rich systems and at temperature below 1600–1800 K [18]. However, the temperature fluctuations in turbulent combustion systems can extend the importance of the Zeldovich mechanism to lower mean temperatures [19]. Nonetheless, because of the low temperature of the fuel-rich pulverized coal flames in W-shaped boilers being considered (which lack oxygen atoms), the Zeldovich mechanism does not appear to be significant source of NO [20]. For this reason, in the present paper, we have used a approximate NO formation model Eq. (15).

The conversion of fuel nitrogen follows a scheme based on known reactions proceeding via the pathways shown in Fig. 1. The nitrogen in the coal is considered to partition between the volatiles and char such that its concentration in the volatiles is identical to that in the dry, ash-free parent coal [21]. Fuel NO formed in the gas-phase results from oxidation of devolatilized nitrogen constituents, and generally accounts for 60–80% of the total NO formed. The nitrogen remaining in the char is converted to gaseous species at a rate proportional to the rate of carbon combus-

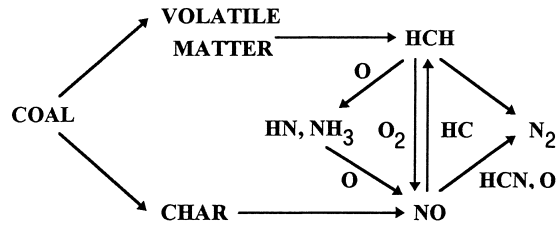

Fig. 1. Reaction scheme for NO_x chemistry.

tion. Regarding the formation of NO from char it is assumed that char nitrogen is released as NO according to the experimental results found by Song et al [22], while the remainder is reduced to N_2. The volatile nitrogen is lost as either HCN or NH_3, which may be secondary products from the pyrolysis of primary tar. These products enter into homogeneous gas-phase reactions as follows

$HCN + O_2 \rightarrow NO + \cdots$ (reaction 3)

$HCN + O \rightarrow NH + CO$ (reaction 4)

$HCN + NO \rightarrow N_2 + \cdots$ (reaction 5)

$NH + O \rightarrow NO + H$ (reaction 6)

$CH + NO \rightarrow HCN + O$ (reaction 7)

$CH_3 + NO \rightarrow HCN + H_2O$ (reaction 8)

The homogeneous gas-phase reactions (reaction 3–8) which influence NO_x emissions involve hydrocarbons from the volatiles, HCN, NH_3 and NO. The time-averaged solution to the transport equation Eq. (1) is adopted for calculating the HCN, NH_3 and NO concentrations. The contributions of fuel nitrogen to the HCN, NO or NH_3 source terms ($i = 1$, 2 or 3) and the contributions of the gas-phase reactions (reaction 3–8) to a source term can be expressed in general form by

$$S_i = A\rho_g^{\alpha} \prod_j Y_j^{\beta} \prod_j M_j^{Y} \exp\left(-\frac{E}{T}\right) \quad (16)$$

Where $\prod$ represents the product of mass fraction Y and molecular masses M of reacting species j etc. The values for the coefficients and exponents used are given in Table 2. The kinetic constants for the gas-phase reaction of the nitrogen species which are listed in Table 2 are taken either from De Soete [3], Glarborg et al. [23] or Miller and Bowman [24].

NO may also be reduced by the char [25]. Chan et al. [26] suggest that NO reduction by this mechanism could make a significant contribution to overall NO reduction, this could be especially true for a low volatile coal that will result in relatively high carbon loading in the furnace coupled with a long residence time. The rate of NO reduction is described as follows

$$W = \alpha_p n_p (4.18 \times 10^7) A_E \rho_{NO} \exp(-34.7/RT) \quad (17)$$

This equation is obtained from measurements in an electrically heated, laminar flow furnace operated in the temperature range of 1250–1750 K with pulverized char in helium carrier gas [27].

3. Application of the numerical code

The model described is applied to a full-scale furnace chamber, which is part of a 300 MW (electrical output) W-shaped utility boiler. A schematic view of the furnace chamber is given in Fig. 2. The geometric parameters of the burners and the operating parameters for two operating conditions are listed in Table 3. A swirl number of 0.6 for burners is considered as a solid rotation in the adjacent inlet velocities. The analysis of the coal used is presented in Table 4. The composition of coal is traditionally characterized by American Society of Testing Materials (ASTM) proximate analysis or ASTM ultimate analysis. The former determines only the moisture content (by drying), percent volatiles (from inert devolatilization at about 1200 K), ash, (residual after complete combustion in air), and fixed carbon (by difference). It is noted that the actual yield of volatiles under combustion conditions is likely to be higher than that determined by a proximate analysis, because some ash components are volatile at higher temperatures. ASTM ultimate analysis gives elemental analyses for carbon, hydrogen, nitrogen, sulfur, and oxygen, the latter often determined by difference. The residual mineral matter is shown as ash. A continuous distribution of coal-particle sizes is represented by using 16 different size classes. The mass fractions for various size classes are shown in Table 5.

The numerical procedure for gas-phase is based on a well-known volume finite discretization of staggered grids, which has been developed by Patankar and Spalding [28]. A five-stage iteration method is used in integrating the conventional difference equations for the coal particles [29]. The simulations are carried out considering half of the furnace

Table 2
Values used in rate expressions Eq. (16)

Reaction	3	4	5	6	7	8
A	1.0×10^{11}	$3.5T^{2.64}$	3.0×10^{12}	$6.38 \times 10^{12}T^{0.5}$	1.0×10^{11}	1.0×10^{8}
α	1	2	1	2	2	2
$Y_1^{\beta_1}$	Y_{HCN}^{1}	Y_{O}^{1}	Y_{HCN}^{1}	Y_{O}^{1}	$Y_{volatiles}^{1}$	$Y_{volatiles}^{1}$
$Y_2^{\beta_2}$	$Y_{O_2}^{b}$	Y_{HCN}^{1}	Y_{NO}^{1}	Y_{NH}^{1}	Y_{NO}^{1}	Y_{NO}^{1}
$M_1^{\gamma_1}$	M_{NO}^{1}	M_{NH}^{1}	$M_{mixture}^{1}$	M_{NO}^{1}	$M_{volatiles}^{-1}$	$M_{volatiles}^{-1}$
$M_2^{\gamma_2}$	M_{HCN}^{-1}	M_{O}^{-1}	M_{HCN}^{-1}	M_{O}^{-1}	–	–
$M_3^{\gamma_3}$	$M_{mixture}^{b}$	M_{HCN}^{-1}	–	M_{HN}^{-1}	–	–
$M_4^{\gamma_4}$	$M_{O_2}^{-b}$	–	–	–	–	–
$E(K)$	33 738	2506	30 214	0	0	7580

Note: the value of b varies between unity and zero, depending on oxygen concentration.

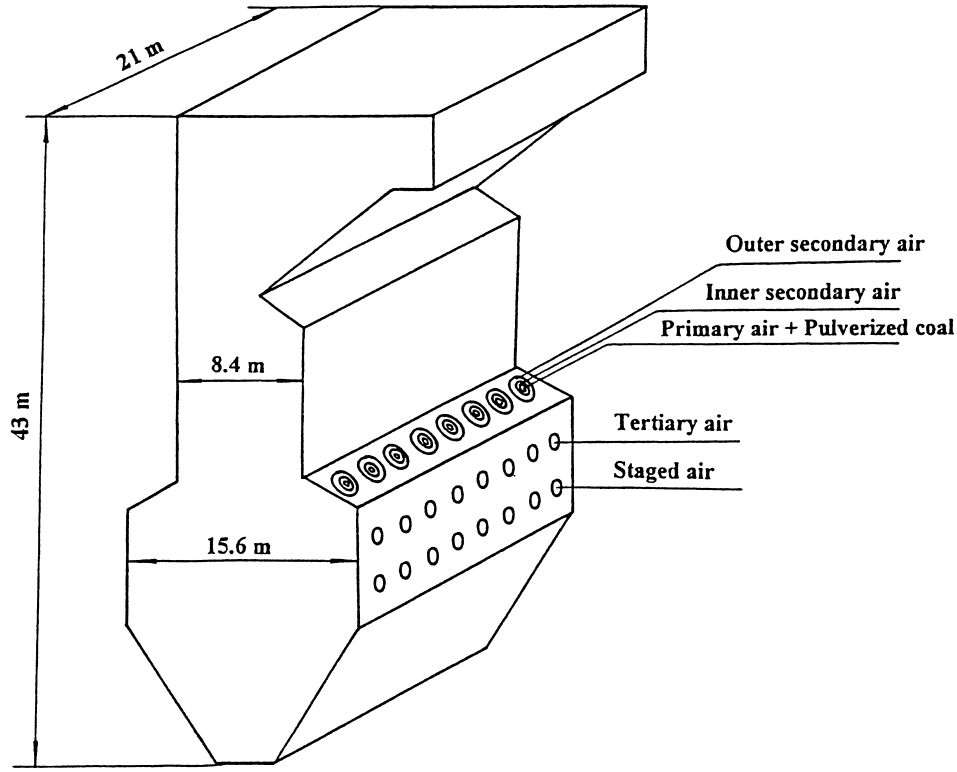

Fig. 2. Schematic view of the 300 MW W-shaped boiler furnace.

Table 3
Nozzle sizes and simulated operating cases

Parameter	Nozzle size (mm)	Full load case		50% load case	
		Velocity (m/s)	Temperature (°C)	Velocity (m/s)	Temperature (°C)
Primary air	550 × 14	17.0	214.8	16.1	191
Coal particle	see Table 4	9.8	25.0	9.8	25
Inner secondary air	951 × 8	20.2	341.0	19.7	299
Outer secondary air	1164 × 6	41.1	341.0	40.0	299
Staged air	382 × 6	38.6	341.0	37.3	299
Tertiary air	482 × 6	22.3	90.0	25.1	90

Table 4
Analysis of coal used

Proximate analysis (%)				Ultimate analysis (ar%)					Heating value (MJ/kg)
MS	Ash	VM	FC	C	H	O	N	S	
6.00	21.82	16.72	55.46	64.89	2.83	2.4	0.98	1.08	28.87

with symmetry conditions at the middle plane using a grid comprising $68\times86\times100$ ($=584\,800$) control volumes. Grid-dependence tests are conducted. The specified grid is fine enough to give grid-independent solutions. Since the numerical code solves the elliptic form of the differential equations, information about the boundary conditions surrounding the domain of interest is required. (i) gas and particle mass, momentum and thermal energy at the inlets of burners are specified, which is given in Table 3. (ii) wall friction is supplied only to the gas. The usual non-slip conditions apply at the furnace wall. To account for the furnace-wall effect in the nearby regions, equations are introduced to link velocities, k and ε at the wall to those in the near-wall region. These equations are called wall

Table 5
The percentage of various size classes of pulverized coal

Particle diameter (μm)	Percentage	Particle diameter (μm)	Percentage
5	20.22	160	1.42
20	28.04	180	0.94
40	17.92	200	0.62
60	11.61	220	0.41
80	7.58	240	0.27
100	4.97	260	0.18
120	3.27	280	0.12
140	2.16	300	0.25

functions and are introduced and used in finite difference calculations at near-wall points. This approach may be a poor approximation in regions where particle concentrations are high. Its net effect would be under prediction of the pressure drop. (iii) heat transfer to the wall occurs through a prescribed heat sink via the gas. Empirical expressions exist for particle-to-wall heat transfer [30]. (iv) finally, a constant pressure boundary is assumed for the furnace exit.

The calculation strategy starts with solving the gas flow-field equations assuming that the particles are absent. Using the flow field, particles' trajectories, their temperature and burn-out histories are determined. The mass, momentum and energy source terms for each cell are calculated. The source terms are included in the gas-phase equations and the flow field is then re-calculated. The process is repeated until further repetition fails to change the solution. Thus, The mutual interaction of the gas and particles is accounted for. The overall convergence is achieved after about 2500–3500 iterations.

4. Results and discussions

The paper presents numerical simulations considering full load and 50% load and their effect on the NO_x emissions. Fig. 3 presents the predicted flow field for two cases in a plane across the burner close to the central of the furnace. The plane which contain burner centerlines is chosen to provide an overview of the chemical species distribution around the burners. The flow is highly tri-dimensional although from the figure two strong recirculating regions can be identified below the burner levels. Primary and secondary air mix with tertiary and staged air in the middle of the lower part of the furnace. The gas flow does not penetrate far before turning upwards, and the W-shaped flow pattern is finally formed. Fig. 4 shows model predictions compared with measurement of velocity distributions of gas-phase in the central vertical plane for the full load case. Agreement between predictions and measurements is reasonably good. Comparison with the velocity

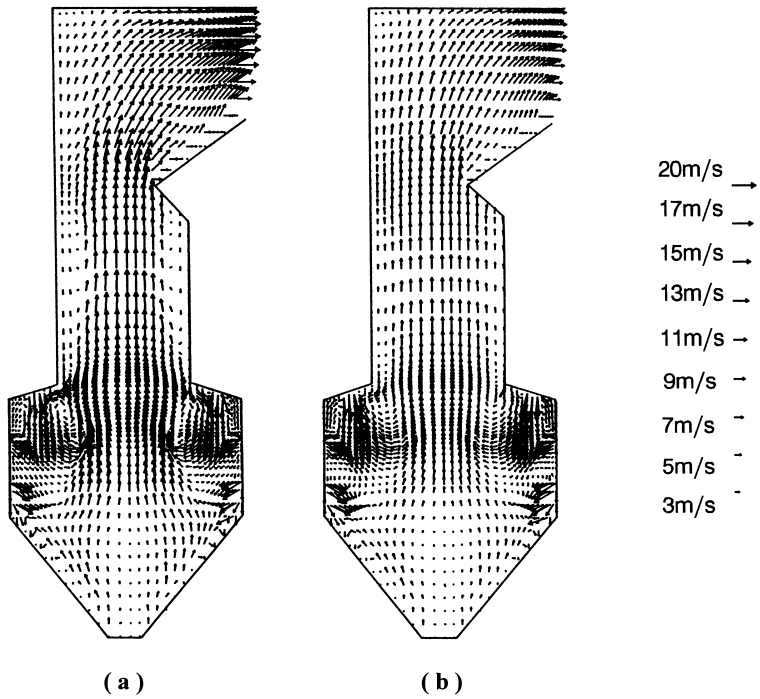

Fig. 3. Predicted flow field in the central vertical plane of the furnace; (a) full load case, (b) 50% load case.

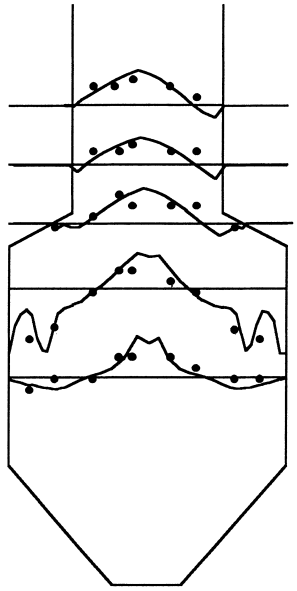

Fig. 4. Predicted and measured gas-phase velocities for full case in the central vertical plane of the furnace (● experimental data; ——— model predictions)

distributions for two cases, the predicated velocity field for 50% load in the central vertical plane of the furnace is similar with that of full load, but the velocity is lower.

Fig. 5 presents contours of the temperature and distributions of the oxygen mass-fraction in the central vertical plane for full load, these figures show the strong relation between the oxygen concentration and temperature distribution. As expected, the higher-temperature regions correspond to low oxygen concentrations. It is observed that the

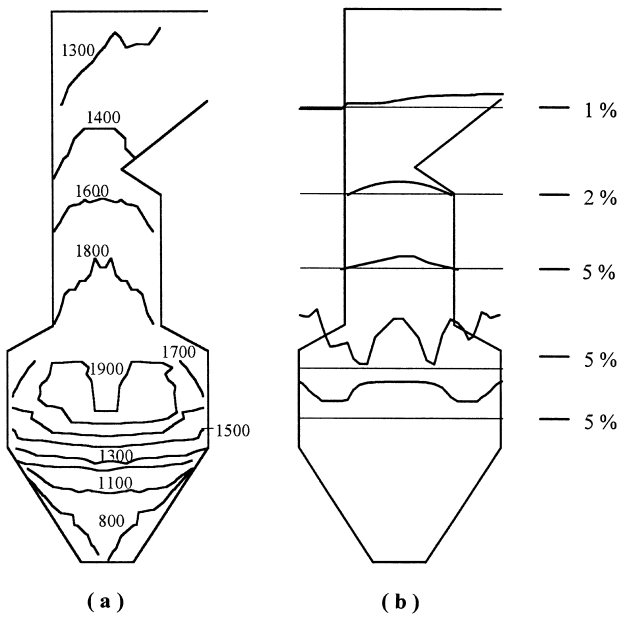

Fig. 5. Predicted contours of temperature and oxygen mass-fraction for full load case in the central vertical place of the furnace; (a) temperature, (b) oxygen mass-fraction.

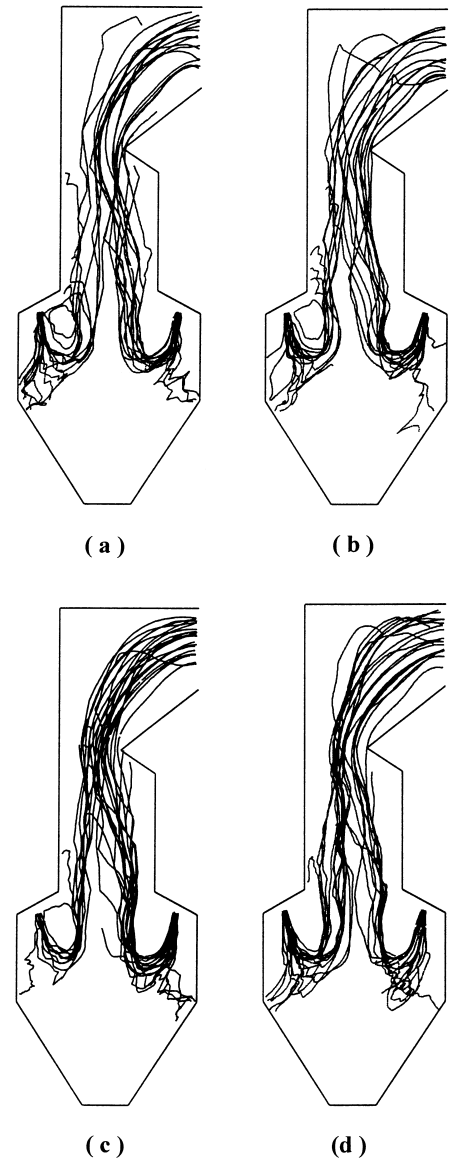

Fig. 6. Some representative predicted trajectories for full load case; (a) $d_p = 40\,\mu m$, (b) $d_p = 80\,\mu m$, (c) $d_p = 120\,\mu m$, (d) $d_p = 160\,\mu m$.

oxygen concentration is relatively high near the burners, whereas the temperature is lower. The oxygen concentration decreases greatly with the jets rushing down because of char combustion. The high-temperature region is formed under the arches. This fact is in agreement with measurements of radiant fluxes made for similar boiler under normal operating conditions. The temperature is between 1700–1900 K which would benefit to the ignition and carbon burn-out, this proves the W-shape flame boiler is suitable for combustion of low quality coal. The highest temperatures occur in a shape of saddle in the central part of the furnace. This can be explained by the alternative coal particle trajectories for this case (see Fig. 6) and by the presence of a region of intensive combustion activity in the middle of the furnace. It leads to very low levels of oxygen concentration in that region as can

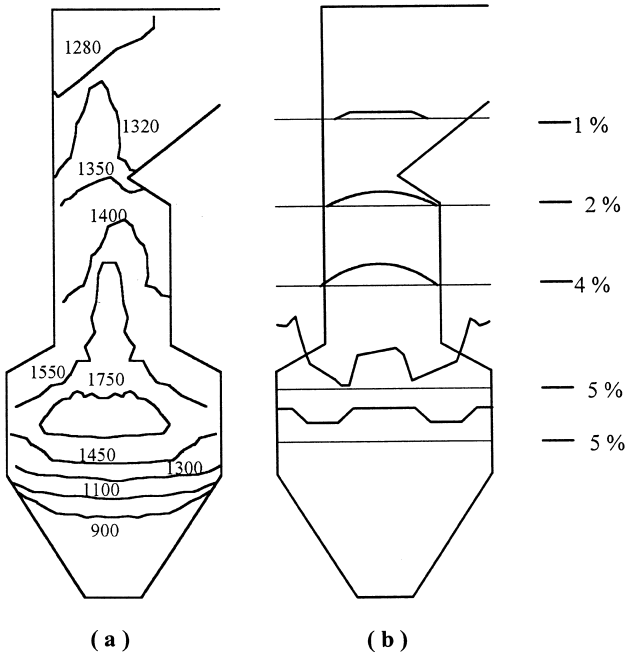

Fig. 7. Predicted contours of temperature and oxygen mass-fraction for 50% load case in the central vertical plane of the furnace; (a) temperature, (b) oxygen mass-fraction.

be seen in that figure. Close to the tertiary and staged air oxygen and staged air jets, oxygen is transported from the unfired air around flames and is mixed with the flames due to the swirl action of the burners.

Fig. 7 shows contours of the temperature and the distributions of oxygen mass-fraction in the central vertical plane for 50% load. Although the flow presents the same overall characteristics as in the case of the full load, coal ignition distance from the burner exit is longer than that of full load because of lower temperature. Combustion is controlled in its early stages by the rates of reaction of the solid residues. The high temperature region occurs in the central part of the furnace similar to that for full load, but the highest temperature is only 1759 K, which is lower than that for full load. Although the oxygen concentration distribution is nearly as the same as for full load, this may be observed in the values of the oxygen concentration for 50% load which shows that only the lower region close to the burners is affected by the partial load.

Using these results, NO_x formation is calculated based on the model mentioned previously. When a basic De Soete model (reaction 3 and 5 – using HCN and NO only) is used, an exit NO_x value of 322 ppm is predicted, which is lower than the measured value of 355 ppm for full load. When ammonia chemistry is added, the predicted exit values of NO_x are too high (415 ppm). When a reburn mechanism (reaction 7, HC) is considered, the exit NO_x of 386 ppm is still too high. If in reaction 8, CH_3 reburn mechanism is used, the exit NO_x is predicted to be 285 ppm, which is too low. However if thermal NO_x is considered, the value increases to 312 ppm. The full NO_x chemistry model, including thermal NO_x, predicted 370 ppm, which is in good agreement with the measured value. Fig. 8 shows the predicted NO_x mass-fraction contours for two cases. Since the fuel-NO_x formation is strongly influenced by oxygen concentration, this species is mostly formed within the envelop of the flames. Coal volatiles are formed in the near-burner region. Both char and volatiles release HCN equally according to De Soete's mechanism. Therefore, in the fuel-rich region of the flames NO_x is formed around the

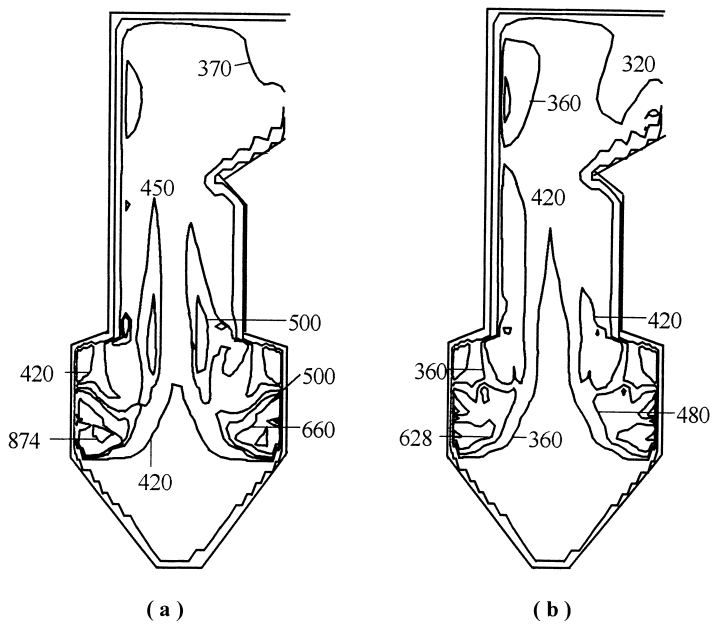

Fig. 8. Predicted NO_x mass-fraction contours for full load case and 50% load case in the central vertical plane of the furnace; (a) full load case; (b) 50% load case.

burners leading to a maximum value of 874 ppm in the region. The oxygen concentration is lower in the center of the flame where the temperature is very high, but the NO_x concentration is not the highest. For the partial load due to the increase of excess air compared with the full load, the NO_x formed from volatiles increases while the contribution from char is more diluted. Comparing the 50% load with the full load the NO_x concentration decreases due to the effective air supply. For 50% load the highest NO_x mass fraction was 628 ppm but was reduced to 320 ppm at the exit.

5. Conclusions

The three-dimensional model describing gas-particle flow, heat transfer and combustion presented here provides reasonable accurate prediction of the distribution of the velocity, temperature and chemical species in good agreement with expected values in a W-shaped boiler furnace. A simple model for nitrogen chemistry has been included in the basic computational fluid dynamics model. The predicted NO_x emissions are slightly overpredicted (about 4% higher comparing with measured values for the full load), but the sensitivity achieved is satisfactory. This suggests that the numerical code may be used with some confidence for design and development calculations of the W-shaped boiler furnaces.

6. Nomenclature

A_E	Arrhenius coefficient
A_p	Coal-particle area
C_D	Drag coefficient
C_g	Gas molar concentration
C_μ, C_1, C_2	Empirically determined constants
D_w	Binary diffusivity
d_p	Particle diameter
E	Activation energy
f	Scalar mixture
g	Time-mean value of square of difference of instantaneous mixture fraction
h	Enthalpy
I	Radiation intensity
K	Reaction-rate coefficient
K_c	Mass-transfer coefficient
K_g	Thermal conductivity of the gas
k	Mean turbulent kinetic energy
L	Latent heat
M	Molecular weight
m_p	Particle mass
Nu	Nusselt number
n_p	Particle number density
Pr	Prandtl number
p	Pressure
Q	Particle-to-gas heat-transfer rate
R	Gas constant
Re	Reynolds number
r	Particle reaction rate
Sc	Schmidt number
S_ϕ	Gas source term for variable 0
$S_{\phi,p}$	Particle source term for 0
t	Time
T	Temperature
u	x-direction velocity
v	y-direction velocity
$\mathbf{v}$	Velocity vector
V	Concentration of volatiles
w	z-direction velocity
x	Coordinate
X	Mole fraction
y	Coordinate
Y_k	Concentration of the kth chemical species
Y	Pyrolysis coefficient
z	Coordinate

Greek letters

α'_{kj}, α''_{kj}	Stoichiometric coefficient of species k in reaction j
ε	Emissivity, or dissipation rate of turbulence
μ	Viscosity
ρ	Density
σ	Stefan-Boltzmann constant
σ_k, σ_ε	Turbulent Prandtl and Schmidt numbers
ϕ	General variable
ϕ_l	Stoichiometric coefficient of the lth reaction
Γ	Effective viscosity

Subscripts

c	Convection of coal
daf	Daf coal
eff	Effective
g	Gas
h	Char
l	Char oxidation reaction
m	Mean
p	Particle
r	Radiation
v	Volatiles
w	Moisture

Acknowledgements

The authors are grateful for support provided by the National Natural Science Foundation of Peoples' Republic of China.

References

[1] A. McConville, Proc. 22nd Int. Tech. Conf. on Coal Utilization and Fuel Systems, in: B. A. Sakkestad (Ed.), Published by Coal and Slurry Technology Association, Washington DC, 1997, pp. 1–12.

[2] J.P. Smart, T. Nakamura, J. Inst. Energy 66 (1993) 99–105.

[3] G.G. De Soete, Overall Reaction Rates of NO and N_2 Formation from Fuel Nitrogen. 15th Int. Symp. on Combustion, The Combustion Institute, Pittsburgh, PA, 1975, 1093–1192.

[4] J.H. Pohl, S.L. Chen, M.P. Heap, D.W. Pershing, Proc. 1982 Joint Symp. Stationary NO_x Control, 1983.

[5] S.M. Smouse, D.J. Wildman, T.S. Mcllvreid, N.S. Harding, Proc. 1993 Joint EPA/EPRI Symp. on Stationary Combustion NO_x Control, 1994.

[6] F.C. Lockwood, C.A. Romo-Millares, Combust. Sci. Technol. 102 (1994) 57–80.

[7] W.A. Fiveland, R.A. Wessel, J. Inst. Energy 64 (1991) 41–54.

[8] F.C. Lockwood, C.A. Romo-Millares, J. Inst. Energy 65 (1992) 144–152.

[9] W.A. Fiveland, C.E. Latham, Combust. Sci. Technol. 93 (1993) 53–72.

[10] C.F.M. Coimbra, J.L.T. Azevedo, M.G. Carvalho, Fuel 73 (1994) 1128–1134.

[11] B. Epple, U. Schnell, Modeling of coal combustion and NO_x formation in industrial furnaces, Int. Joint Power Generation Conf., ASME Paper, Atlanta, USA, 1992.

[12] B. Epple, H. Bruggemann, A. Kather, Proc. of the 3rd Int. Symp. on Coal Combustion, in: X.C. Xu, L.X. Zhou (Eds.), Science Press, Beijing, China, 1995, pp. 553–560.

[13] L.R. Coelho, J.L.T. Azevedo, M.G. Carvalho, Proc. of the 3rd Int. Symp. on Coal Combustion, in: X.C. Xu, L.X. Zhou (Eds.), Science Press, Beijing, China, 1995, pp. 617–624.

[14] D.B. Spalding, Combustion and Mass Transfer, Pergamon Press, London, 1979.

[15] J.M. Hammersley, D.C. Handscomb, Monte Carlo Methods, John Wiley & Sons Inc., New York, 1964.

[16] J.R. Fan, X.Y. Zhang, L.H. Chen, K.F. Cen, Chem. Eng. J. 66 (1997) 215–297.

[17] W.B. Fu, Y.P. Zhang, H.G. Han, Y.N. Duan, Combust. Flame 70 (1987) 253.

[18] P.C. Malte, D.T. Pratt, Combust. Sci. Tech. 9 (1974) 221.

[19] A.N. Hayhwrst, I.M. Vince, Prog. Energy Combust. Sci. 6 (1980) 35.

[20] J.O.L. Wendt, Prog. Energy Combust. Sci. 6 (1980) 201.

[21] W. Wand, S.D. Brown, C.J. Hindmarsh, K.M. Thomas, Fuel 73 (1994) 1381–1388.

[22] Y.H. Song, J.H. Pohl, J.M. Beer, A.F. Sarofim, Combust. Sci. Technol. 28 (1982) 31–39.

[23] P. Glarborg, J.A. Miller, R.J. Knee, Combust. Flame 65 (1986) 177–202.

[24] J.A. Miller, C.T. Bowman, Prog. Energy Combust. Sci. 15 (1989) 287–338.

[25] M.R. Lery, L.K. Chan, A.K. Sarofim, J.M. Beer, NO/char reactions at pulverized coal flame conditions. 18th Int. Symp. on Combustion, The Combustion Institute, Pittsburgh, PA, 1981, 111.

[26] L.K. Chan, A.F. Sarofim, J.M. Beer, Combust. Flame 52 (1983) 37–45.

[27] L.D. Smoot, P.J. Smith, Coal Combustion and Gasification, Plenum Press, New York, 1985.

[28] S.V. Patankar, D.B. Spalding, Int. J. Heat Mass Trans. 15 (1972) 1787.

[29] J.R. Fan, X.H. Liang, Q.S. Xu, X.Y. Zhang, K.F. Cen, Energy 22 (1997) 847–857.

[30] J.S.M. Botterill, Fluidized Bed Heat Transfer, Academic Press, London, 1975.